Preprints of the 19th World Congress
The International Federation of Automatic Control
Cape Town, South Africa. August 24-29, 2014

Combined Estimation of Friction and Patient Activity in Rehabilitation Robotics

T. Specker * **M. Buchholz** * **K. Dietmayer** *

* *Institute of Measurement, Control and Microtechnology, University of Ulm, D-89081 Ulm, Germany (e-mail: thomas.specker@uni-ulm.de, michael.buchholz@uni-ulm.de, klaus.dietmayer@uni-ulm.de)*

Abstract: Robot-assisted gait training has shown promising results in inpatient rehabilitation. However, the progress the patients can achieve during this period often stagnates or even deteriorates after their discharge. To extend the robot-assisted gait training to the patient's home area, a new rehabilitation robot is developed. Since the home training is not supervised by physiotherapists, a challenging training is needed as well as a reliable and comprehensible feedback to the patient. Therefore, the patient activity has to be estimated and set apart from the occurring friction forces falsifying the estimation. In this paper, an approach is described that offers a combined estimation of friction forces and patient activity, based on a new dynamic friction model and a central difference Kalman filter.

Keywords: Robotics; Medical systems; Kalman filters; State observers; Friction.

1. INTRODUCTION

Robotic devices are essential elements in today's rehabilitation of patients with neuromuscular gait disorders. As proposed in Kakabeeke et al. (2006), an improvement of the capability to walk can only be achieved by an intense training with high repetition rates. Since manually training assisted by physiotherapists is hard work, it is more and more supplemented by robotic devices to increase the intensity to a sufficient amount. In the inpatient rehabilitation, the usage of huge, complex, and expensive robots has been enforced with positive influence on the walking capabilities of the patients, as was shown in Wirz et al. (2005).

After the inpatient phase, it is often not possible to maintain the extensive gait training and the former achieved progress stagnates or even deteriorates. Thus, it was obvious to extend the robotic gait training to the patient's home area. In a first approach described in Knestel (2010) and evaluated in Rupp et al. (2011), it was shown that the robot assisted training at home leads to a significant improvement of walking speed and stamina of chronic patients with incomplete spinal cord injuries.

Based on these promising results, a follow-up project was started and the gait trainer was revised. It was necessary to replace the formerly used pneumatic muscles by electric drives, which are easier to maintain. Furthermore, a more realistic gait pattern was requested by the patients. Thus, the concept of the new gait trainer, shown in Fig. 1, has considerably changed. Due to reasons of safety, the patient is still arranged in a half-lying position and tied to the exoskeleton of the rehabilitation robot by three orthosis. The gait trainer is able to simulate an almost natural gait, concerning the hip, knee, and ankle trajectories, with only two degrees of freedom defined by the hip angle and the position of the linear slide below the foot. For relieving the electric drives, the drive units are supplemented by springs that compensate the weight of the exoskeleton and the human leg. Since a good gait approximation is not sufficient to trigger the effect of motor learning based on neuroplasticity without the weight load on the feet that occurs at the roll-over from heel to strike, the gait trainer is supplemented by a stimulative shoe unit.

The combination of a good gait approximation with the stimulative shoe is a promising basis for a successful rehabilitation, but due to the fact that the gait trainer is used without supervision by a physiotherapist, there are other requirements that have to be considered. The training device should be save and easy to operate, challenging to keep the patient motivated, and able to offer a reliable and comprehensible feedback to the patient.

As a basis for adaptive control and feedback, the influence of the patient on the gait trainer has to be estimated. This can be done using a state observer based on the system model extended by a disturbance model. If the dynamic behaviour of the disturbance is unknown, it is common to replace it by a simple integrator model that aggregates all occurring disturbances into as many states as system inputs.

In the case of the new gait trainer, the application of a simple integrator model would lead to an undesired side effect. Since the integrator model summarizes all disturbances, it cannot distinguish between the patient activity and the occurring friction forces, which are in this case very high due to transmission losses and the usage of slide bearings. To set the patient activity apart from the friction forces, another disturbance model has to be used that approximates the friction in an adequate accuracy and that is applicable with a non-linear state observer.

Copyright © 2014 IFAC

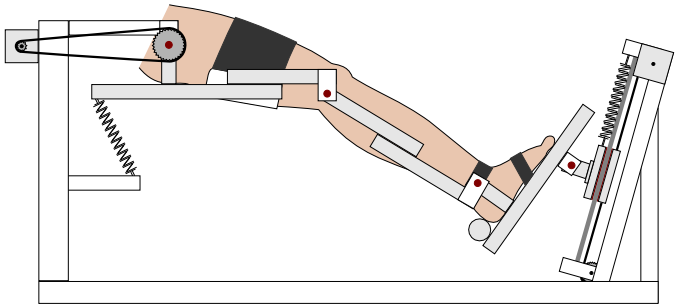

Fig. 1. Sketch of the gait trainer with human leg in the sagittal plane.

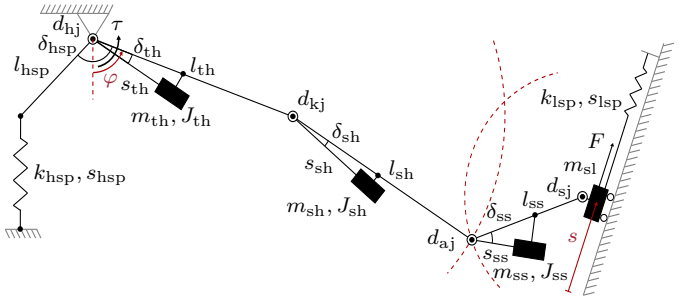

Fig. 2. Schematic view of the rehabilitation robot with masses m, moments of inertia J, lengths l and s, offset angles δ, spring flexibilities k, damping coefficients d, hip torque τ, slide force F, and indices for **th**igh, **sh**ank, **s**timulative **s**hoe, **sl**ide, **h**ip **j**oint, **k**nee **j**oint, **a**nkle **j**oint, **s**lide **j**oint, **h**ip **sp**ring, and **l**inear **sp**ring.

In this contribution, an approach is proposed which enables a precise estimation of the dynamic states of the system model, the values of two dominating friction forces, and the influence of the patient at the same time and with high accuracy. It is based on a dynamic friction model proposed in Specker et al. (2014) and a Central Difference Kalman Filter (CDKF) as described by van der Merwe (2004) and Fox (2007).

The paper is structured as follows: The overall system model is aggregated from three submodels, which are derived and combined to the overall model in Section 2. In Section 3, the CDKF is introduced and completed by the applied algorithm given in Appendix A. The results retrieved by the application of the overall model and the CDKF on a prototype of the gait trainer are presented in Section 4. The paper closes with conclusions and an outlook on further work in Section 5.

2. MODELLING

To obtain an accurate overall system model for state observation, three submodels are presented in the following: a submodel of the rehabilitation robot including minor friction effects, an additional friction submodel describing the major friction effects which cannot be regarded within Lagrangian mechanics, and a simple integrator submodel summing up the disturbances due to the patient activity. Finally the submodels are combined to the overall model.

2.1 Rehabilitation Robot Submodel

For modelling, the construction of the gait trainer, which is depicted in Fig. 1, can be simplified to the schematic view shown in Fig. 2. The system has two degrees of freedom and thus two generalised coordinates, the hip joint angle φ and the position of the slide s, summarized in

$$\boldsymbol{q} = \begin{bmatrix} \varphi \\ s \end{bmatrix}. \tag{1}$$

Based on the generalised coordinates $\boldsymbol{q}$, their first derivatives $\dot{\boldsymbol{q}}$, and the constructive conditions, the position and velocity functions for all masses can be derived. The functions for the thigh profile and the slide depend on one coordinate only and are therefore simple to calculate. The terms for the shank profile and the stimulative shoe depend on both variables and are based on the calculation of the intersection of to circles with moving center points, as depicted in Fig. 2. This makes them more complex and requires a simplification of the model which is described below.

Since all positions and velocities are known, it is possible to calculate the overall energy of the system, distinguished between kinetic energy

$$T = T_{\mathrm{th}} + T_{\mathrm{sh}} + T_{\mathrm{ss}} + T_{\mathrm{sl}} \tag{2}$$

and potential energy

$$V = V_{\mathrm{th}} + V_{\mathrm{sh}} + V_{\mathrm{ss}} + V_{\mathrm{sl}} + V_{\mathrm{hsp}} + V_{\mathrm{lsp}} \tag{3}$$

as well as the minor dissipative energies

$$D = D_{\mathrm{hj}} + D_{\mathrm{kj}} + D_{\mathrm{aj}} + D_{\mathrm{sj}} \tag{4}$$

caused by the friction in the ball bearing mounted joints and described by terms of linear damping. The kinetic and potential energy can be aggregated to the Lagrangian

$$L = T - V. \tag{5}$$

Applying the Euler-Lagrange equation

$$\frac{\mathrm{d}}{\mathrm{d}t}\frac{\partial L}{\partial \dot{q}_i} - \frac{\partial L}{\partial q_i} + \frac{\partial D}{\partial \dot{q}_i} = 0 \quad \text{with} \quad i = 1, 2 \tag{6}$$

yields the non-linear system of differential equations

$$\boldsymbol{M}(\boldsymbol{q})\ddot{\boldsymbol{q}} + \boldsymbol{C}(\boldsymbol{q}, \dot{\boldsymbol{q}})\dot{\boldsymbol{q}} + \boldsymbol{g}(\boldsymbol{q}) = \boldsymbol{0}, \tag{7}$$

with the mass and inertia matrix $\boldsymbol{M}$, the Coriolis, centrifugal, and dissipation matrix $\boldsymbol{C}$ and the potential force and torque vector $\boldsymbol{g}$.

The Coriolis and centrifugal terms considered in $\boldsymbol{C}$ depend on the calculation of the Hessian matrices for all position functions, including those for the shank profile and the stimulative shoe. As already mentioned, these functions are complex to calculate and a second order partial derivative leads to a strong increase of the computational costs. Since the occurring angular velocities are rather small, the Coriolis and centrifugal terms can be omitted with no significant falsification of the overall accuracy, yielding the matrix $\tilde{\boldsymbol{C}}$ comprising dissipative terms only.

The linear slide force F and the the hip torque τ effect the system in the same direction as the generalised coordinates are defined, thus they are equal to the generalised forces

$$\boldsymbol{Q} = \begin{bmatrix} \tau \\ F \end{bmatrix}. \tag{8}$$

Neglecting Coriolis and centrifugal terms and extending the system of differential equations with the generalised forces, the submodel of the rehabilitation robot yields

$$\boldsymbol{M}(\boldsymbol{q})\ddot{\boldsymbol{q}} + \tilde{\boldsymbol{C}}(\boldsymbol{q}, \dot{\boldsymbol{q}})\dot{\boldsymbol{q}} + \boldsymbol{g}(\boldsymbol{q}) = \boldsymbol{Q}, \tag{9}$$

which can be transformed into a system of non-linear first-order differential equations

$$\begin{bmatrix}\dot{\boldsymbol{q}}\\ \ddot{\boldsymbol{q}}\end{bmatrix} = \boldsymbol{f}_\mathrm{r}\left(\boldsymbol{q}, \dot{\boldsymbol{q}}, \boldsymbol{Q}\right). \tag{10}$$

Since the resulting equations are too extensive to be enlisted, they have to be omitted in this contribution.

2.2 Dynamic Friction Submodel

Apart from the viscous friction effects, which are already considered in the robot submodel, there are two remaining friction forces with a significant influence on the overall system, which are caused by the transmission of the hip drive and the bearings of the linear slide. Since those two dissipative forces are based on the effects of Coulomb and Stribeck friction, they cannot be described in an accurate manner using Lagrangian mechanics. Therefore, an additional submodel is proposed based on a dynamic friction model described in Specker et al. (2014).

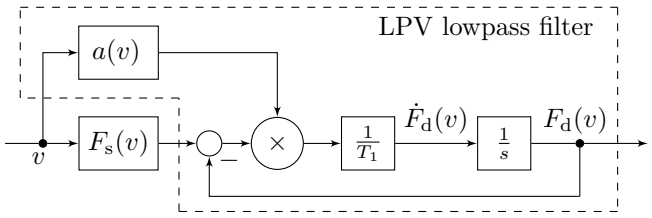

Fig. 3. Block diagram of the dynamic friction model as a serial connection of the static friction model F_s and the adaptive first-order lowpass filter.

The dynamic friction submodel consists of a static friction model with smooth force transitions at standstill and a linear parameter-varying (LPV) first-order lowpass filter. It is based on continuous functions only, which offers numeric stability for high sample times and makes it applicable with non-linear observer approaches like the CDKF described in section 3. The dynamic behaviour of the friction model is defined by the differential equation

$$\dot{F}_\mathrm{d}(v) = \frac{a(v)}{T_1}\left(F_\mathrm{s}(v) - F_\mathrm{d}(v)\right) = f_\mathrm{d}(v) \tag{11}$$

with time constant T_1, edge velocity v_0, adaption factor

$$a(v) = 1 - \mathrm{e}^{-\left(\frac{v}{v_0}\right)^2} \tag{12}$$

and the static friction model output

$$F_\mathrm{s}(v) = \underbrace{\left(\hat{F}_\mathrm{s} - \hat{F}_\mathrm{c}\tanh\left(\frac{v_\mathrm{sp}}{v_\mathrm{t}}\right) - dv_\mathrm{sp}\right)\frac{v}{v_\mathrm{sp}}\,\mathrm{e}^{-\left(\frac{v}{\sqrt{2}v_\mathrm{sp}}\right)^2+\frac{1}{2}}}_{\text{Stribeck friction}} + \underbrace{\hat{F}_\mathrm{c}\tanh\left(\frac{v}{v_\mathrm{t}}\right)}_{\text{Coulomb friction}} + \underbrace{dv}_{\text{Viscous friction}}. \tag{13}$$

The behaviour of the static friction model is defined by the linear damping factor d, the Coulomb force $\hat{F}_\mathrm{c}$, the transition velocity v_t, the Stribeck force $\hat{F}_\mathrm{s}$, and the Stribeck peak velocity v_sp. A detailed description of the single parameters and their effects on the model behaviour is given in Specker et al. (2014).

Since there are two dominating friction sources in the rehabilitation robot that have to be considered in the overall model, the robot's friction submodel consists of two independent non-linear first-order differential equations of the form (11):

$$\dot{\tau}_\mathrm{d,fr} = f_\mathrm{d,hip}\left(\tau_\mathrm{d,fr}, \dot{\varphi}\right), \tag{14}$$

$$\dot{F}_\mathrm{d,fr} = f_\mathrm{d,slide}\left(F_\mathrm{d,fr}, \dot{s}\right). \tag{15}$$

They describe the behaviour of the friction torque $\tau_\mathrm{d,fr}$ in the transmission of the hip drive and the friction force $F_\mathrm{d,fr}$ caused by the slide bearings. Both equations depend on their particular velocities, which are equal to the generalised velocities in $\dot{\boldsymbol{q}}$.

2.3 Integrator Disturbance Submodel

The remaining disturbance effects based on the patient activity are described by a linear integrator disturbance submodel consisting of two independent integrators. Each integrator summarizes all occurring disturbances belonging to one generalised force. For this application, the state variables of the model are chosen in the same manner as the drive forces effect the system. Thus, the dynamics of the disturbance submodel is represented by the differential equations

$$\dot{\tau}_\mathrm{d,i} = 0 \tag{16}$$

$$\dot{F}_\mathrm{d,i} = 0 \tag{17}$$

with the disturbance torque $\tau_\mathrm{d,i}$ occurring at the hip drive and the disturbance force $F_\mathrm{d,i}$ occurring at the slide drive.

2.4 Overall Model

The three submodels can be aggregated to a non-linear state-space model of order eight with the state variables

$$\boldsymbol{x} = \left[\varphi\ s\ \dot{\varphi}\ \dot{s}\ \tau_\mathrm{d,fr}\ F_\mathrm{d,fr}\ \tau_\mathrm{d,i}\ F_\mathrm{d,i}\right]^\intercal, \tag{18}$$

the two system inputs defined by

$$\boldsymbol{u} = \left[\tau\ F\right]^\intercal, \tag{19}$$

and the system outputs

$$\boldsymbol{y} = \left[\varphi\ s\right]^\intercal. \tag{20}$$

To receive the dynamics of the overall model, the dynamics of the different submodels have to be connected to each other.

The forces and torques of the friction and the disturbance submodels defined by (14)-(17) effect the submodel of the rehabilitation robot defined by (10) in the same way as the generalised forces (8). Therefore, the dynamics of the robot submodel can be extended to

$$\begin{bmatrix}\dot{\boldsymbol{q}}\\ \ddot{\boldsymbol{q}}\end{bmatrix} = \boldsymbol{f}_\mathrm{r}\left(\boldsymbol{q}, \dot{\boldsymbol{q}}, \boldsymbol{Q} + \begin{bmatrix}\tau_\mathrm{d,i} - \tau_\mathrm{d,fr}\\ F_\mathrm{d,i} - F_\mathrm{d,fr}\end{bmatrix}\right) = \tilde{\boldsymbol{f}}_\mathrm{r}\left(\boldsymbol{x}, \boldsymbol{u}\right). \tag{21}$$

The dynamics of the friction model are already dependent on the generalised velocities $\dot{\boldsymbol{q}}$ of the rehabilitation robot and they are independent of the disturbance model. So, (14) and (15) can be aggregated to

$$\boldsymbol{f}_\mathrm{d}\left(\boldsymbol{x}\right) = \begin{bmatrix} f_\mathrm{d,hip}\left(\tau_\mathrm{d,fr}, \dot{\varphi}\right)\\ f_\mathrm{d,slide}\left(F_\mathrm{d,fr}, \dot{s}\right)\end{bmatrix} \tag{22}$$

without any changes. Since the dynamics of the disturbance model is independent from the other models, the overall model can finally be written in the following non-linear state-space representation:

$$\dot{\boldsymbol{x}} = \boldsymbol{f}\left(\boldsymbol{x}, \boldsymbol{u}\right) = \begin{bmatrix}\tilde{\boldsymbol{f}}_\mathrm{r}\left(\boldsymbol{x}, \boldsymbol{u}\right)\\ \boldsymbol{f}_\mathrm{d}\left(\boldsymbol{x}\right)\\ \boldsymbol{0}\end{bmatrix}, \quad \boldsymbol{y} = \boldsymbol{h}(\boldsymbol{x}) = \begin{bmatrix}x_1\\ x_2\end{bmatrix}. \tag{23}$$

3. CENTRAL DIFFERENCE KALMAN FILTER

Kalman filters belong to the most common observer approaches for state estimation in non-linear systems. Especially the extended Kalman filter (EKF), which is based on the linearisation of the underlying non-linear system model, is used in many practical applications. With respect to the overall model proposed in the previous section, the EKF has two disadvantages. As mentioned in Section 2.1, the Coriolis and centrifugal terms of the shank profile and the stimulative shoe are omitted because of their complex and huge terms based on the second partial derivation. If an EKF is used, those terms would have to be calculated due to the required linearisation. Furthermore, it is shown in Specker et al. (2014) that the friction model proposed in Section 2.2 is more precise using a steeper force transition at standstill, but linearising a steep transition can cause numeric problems and, therefore, should be avoided.

Another Kalman filter with growing popularity is the unscented Kalman Filter (UKF) belonging to the class of sigma point Kalman filters (SPKF). SPKFs approximate the probability density of the state estimation with characteristic points, the so-called sigma points. For SPKFs, a partial derivative of the underlying model is not needed and, as mentioned in van der Merwe (2004), they are expected to require less computational costs than EKFs while offering a higher estimation accuracy. Thus, an SPKF is a good choice to be applied to the overall model derived in Section 2.

Since the commonly used UKF has a big set of parameters that has to be chosen, the CDKF, a closely related SPKF, is used in this contribution. It is mentioned in Fox (2007) that in comparison to the UKF, the CDKF shows an equal performance in all practical purposes, but has the advantage of a lower parameter count of the algorithm. A description of the used CDKF algorithm is given in the Appendix A.

4. APPLICATION RESULTS

To evaluate the combined estimation approach distinguishing between friction forces and patient activity, the overall model proposed in Section 2 and the CDKF described in Section 3 and Appendix A are combined for the usage on a real-time linux system which controls the rehabilitation robot and is executed with a rather high sample time of $T_s = 10$ ms.

The data shown in Fig. 4 and Fig. 5 were retrieved from a prototype of the new gait trainer and are evaluated for one leg of the exoskeleton. The disturbances normally caused by a patient are simulated by artificial disturbances to make a quantitative evaluation of the observer accuracy possible. For recording the results, the rehabilitation robot was operated in open-loop effected by sinusoidal actuating variables.

The application data belonging to the hip variables are shown in Fig. 4, containing the actuating variables effecting the hip drive as well as the falsified hip torque seen by the observer, the measured and the estimated hip angle, the estimated velocity in comparison to the numeric derivative of the hip angle, the estimated friction torque, and a comparison between the estimated disturbance torque and the preset disturbance torque calculated by subtracting the actuating variable seen by the observer from the one effecting the robot.

At the beginning, the torque of the hip drive remains zero and the gait trainer is only effected by the linear slide. After 2 s, the drive torque steps to a random value enhancing a velocity peak. Even for this short velocity peak, the dynamic behaviour of the observer is fast enough to follow. Nonetheless, the magnification of the hip velocity shows also a good noise filtering.

The torque step is followed by a sinusoidal torque trajectory maintained to the end of the regarded time period. In the time slot between 2 s and 15 s, there are no disturbances effecting the hip and all state variables are estimated in an accurate manner. When the hip is moving, the value of the estimated friction torque is approximately equal to the determined Stribeck and Coulomb torques, whereas at standstill, it is somewhere in between due to the memory effect of the friction model. The transition between lowpass behaviour and memory effect can be seen in the magnification.

Beginning at 15 s, an artificial disturbance is added to the drive torque seen by the observer, which is simulating the patient activity and changing the characteristic of the actuator variable significantly. As can be seen, there is almost no change in the estimated values except for the state variable describing the disturbances. The disturbance estimation shows a good approximation of the preset disturbance trajectory and, therefore, it should be possible to achieve a satisfying estimation of the patient activity as well.

The application data belonging to the slide variables are shown in Fig. 5 and arranged in the same manner as the hip variables. The slide is effected by a continuous sinusoidal force trajectory moving the slide back and forth.

The friction effect in the linear slide is significantly higher than the hip friction, yielding longer periods at standstill. In case of standstill, the friction submodel changes its behaviour to an integrator as well, therefore, there are two disturbance models with equal model dynamics.

Since the process noise covariance of the friction model is chosen much higher than the process noise covariance of the disturbance model, the estimation of the friction state has a higher dynamic and, therefore, absorbs the simulated disturbance force beginning at 10 s as well. However, there is no standstill occurring in the trajectories of the hip angle and the slide position for the gait training and, therefore, this effect should not appear in closed-loop control. As soon as the slide starts to move again, the value of the estimated friction force decreases to its usual value and the disturbance force is transferred to the desired state variable. At the moment the artificial disturbance disappears, the slide is moving and the friction state shows no significant changes.

Apart from this, the estimation of the state variables at the linear slide shows the same good results as the estimation of the hip variables, consisting of a high accuracy, a good noise filtering, and a sufficient dynamic. Furthermore, a

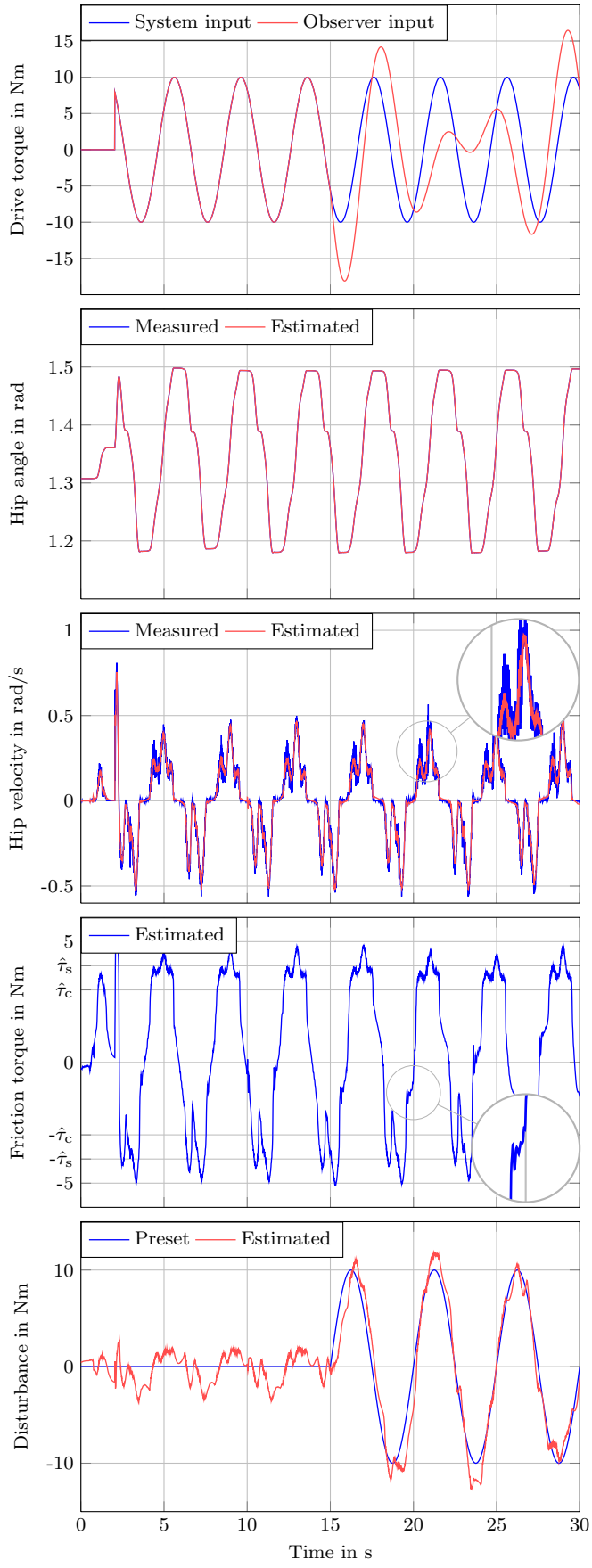

Fig. 4. Estimation results at the hip.

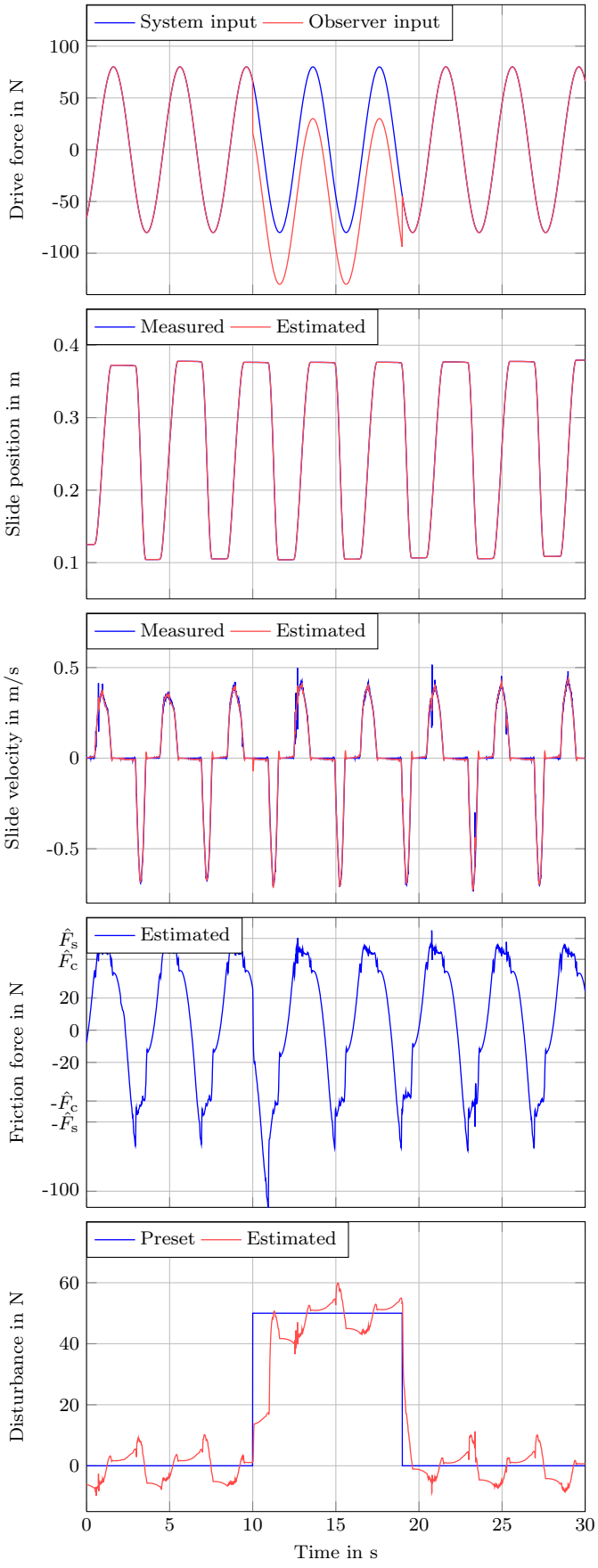

Fig. 5. Estimation results at the linear slide.

cross-connection between hip and slide disturbances is not visible.

5. CONCLUSION

In this contribution, a combined friction disturbance and patient activity estimation approach for a gait rehabilitation robot has been proposed. The method is based on an overall system model including a dynamic friction model based on Specker et al. (2014). This friction model was specially designed for numerical stability even with high sample times. The applicability and usefulness of this friction model was shown in this paper on a relevant practical application, where a CDKF was used as a real-time observer with a relatively high sample time. This setup shows very good results for the patient activity and thus also the friction forces, what was shown with real measurements from a prototype of the training robot.

The next steps will include closed-loop control of the gait rehabilitation robot for an assist-as-needed functionality and an adequate training feedback, both based on the estimated patient activity.

ACKNOWLEDGEMENTS

The authors thank the German Federal Ministry of Economics and Technology for supporting this work through the Central Innovation Program SME within the project KF2648502NT1.

Appendix A. ALGORITHM OF THE CENTRAL DIFFERENCE KALMAN FILTER

The following description of the algorithm is based on the work of Fox (2007). A detailed derivation of SPKFs can be found in van der Merwe (2004). The CDKF works with a predictor-corrector structure. In the time update step, the model-based predictor calculates a state vector $\hat{\boldsymbol{x}}_{k+1}^-$ (model simulation for one time step), which is corrected with measurements from the observed system in the measurement update to $\hat{\boldsymbol{x}}_{k+1}^+$. The time update equation $\boldsymbol{f}(\cdot)$ and measurement update equation $\boldsymbol{g}(\cdot)$ are evaluated $i = 2\,n + 1$ times (where n is the model order) in the so-called sigma points $\boldsymbol{\chi}_{i,k+1}$ to approximate the non-linearities.

Algorithm:

Initialization:

$$\hat{\boldsymbol{x}}_0 = \mathrm{E}\{\boldsymbol{x}_0\}$$
$$\boldsymbol{S}_{\boldsymbol{x},0} = \mathrm{chol}\{\mathrm{E}\{(\boldsymbol{x}_0 - \hat{\boldsymbol{x}}_0)(\boldsymbol{x}_0 - \hat{\boldsymbol{x}}_0)^\intercal\}\}$$

Calculation of sigma points for time update:

$$\boldsymbol{\chi}_{0,k+1}^- = \hat{\boldsymbol{x}}_k^+$$
$$\boldsymbol{\chi}_{i,k+1}^- = \hat{\boldsymbol{x}}_k^+ + h\left(\boldsymbol{S}_{\boldsymbol{x},k}^+\right)_{:,i}$$
$$\boldsymbol{\chi}_{i+n,k+1}^- = \hat{\boldsymbol{x}}_k^+ - h\left(\boldsymbol{S}_{\boldsymbol{x},k}^+\right)_{:,i}$$

Time update:

$$\boldsymbol{\chi}_{i,k+1}^p = \boldsymbol{f}(\boldsymbol{\chi}_{i,k+1}^-, \boldsymbol{u}_k, \boldsymbol{0})$$
$$\hat{\boldsymbol{x}}_{k+1}^- = \frac{h^2 - n}{h^2}\boldsymbol{\chi}_{0,k+1}^p + \frac{1}{2h^2}\sum_{i=1}^{2n}\boldsymbol{\chi}_{i,k+1}^p$$
$$\boldsymbol{S}_{\boldsymbol{x}}^{(1)} = \frac{1}{2h}\left\{\boldsymbol{\chi}_{i,k+1}^p - \boldsymbol{\chi}_{i+n,k+1}^p\right\}_{i=1,\ldots,n}$$
$$\boldsymbol{S}_{\boldsymbol{x}}^{(2)} = \frac{\sqrt{\sigma_4 - 1}}{2h^2}\left\{\boldsymbol{\chi}_{i,k+1}^p + \boldsymbol{\chi}_{i+n,k+1}^p - 2\boldsymbol{\chi}_{0,k+1}^p\right\}_{i=1,\ldots,n}$$
$$\boldsymbol{S}_{\boldsymbol{x},k+1}^- = \mathrm{QR}\left\{\left(\boldsymbol{S}_{\boldsymbol{x}}^{(1)}\ \ \boldsymbol{S}_{\boldsymbol{x}}^{(2)}\ \ \sqrt{\boldsymbol{Q}_\mathrm{w}}\right)\right\}$$

Calculation of sigma points for measurement update:

$$\boldsymbol{\chi}_{0,k+1}^+ = \hat{\boldsymbol{x}}_{k+1}^-$$
$$\boldsymbol{\chi}_{i,k+1}^+ = \hat{\boldsymbol{x}}_{k+1}^- + h\left(\boldsymbol{S}_{\boldsymbol{x},k+1}^-\right)_{:,i}$$
$$\boldsymbol{\chi}_{i+n,k+1}^+ = \hat{\boldsymbol{x}}_{k+1}^- - h\left(\boldsymbol{S}_{\boldsymbol{x},k+1}^-\right)_{:,i}$$

Measurement update:

$$\boldsymbol{\mathcal{Y}}_{i,k} = \boldsymbol{g}(\boldsymbol{\chi}_{i,k+1}^+, \boldsymbol{u}_k, \boldsymbol{0})$$
$$\hat{\boldsymbol{y}}_{k+1}^- = \frac{h^2 - n}{h^2}\boldsymbol{\mathcal{Y}}_{0,k} + \frac{1}{2h^2}\sum_{i=1}^{2n}(\boldsymbol{\mathcal{Y}}_{i,k})$$
$$\boldsymbol{S}_{\boldsymbol{y}}^{(1)} = \frac{1}{2h}\left\{(\boldsymbol{\mathcal{Y}}_{i,k} - \boldsymbol{\mathcal{Y}}_{i+n,k})\right\}_{i=1,\ldots,n}$$
$$\boldsymbol{S}_{\boldsymbol{y}}^{(2)} = \frac{\sqrt{\sigma_4 - 1}}{2h^2}\left\{(\boldsymbol{\mathcal{Y}}_{i,k} + \boldsymbol{\mathcal{Y}}_{i+1,k} - 2\boldsymbol{\mathcal{Y}}_{0,k})\right\}_{i=1,\ldots,n}$$
$$\boldsymbol{S}_{\boldsymbol{y},k+1}^- = \mathrm{QR}\left\{\left(\boldsymbol{S}_{\boldsymbol{y}}^{(1)}\ \ \boldsymbol{S}_{\boldsymbol{y}}^{(2)}\ \ \sqrt{\boldsymbol{R}_\mathrm{w}}\right)\right\}$$
$$\hat{\boldsymbol{P}}_{\boldsymbol{xy},k+1}^- = \boldsymbol{S}_{\boldsymbol{x},k+1}^-(\boldsymbol{S}_{\boldsymbol{y}}^{(1)})^\intercal$$
$$\boldsymbol{K}_{k+1} = \hat{\boldsymbol{P}}_{\boldsymbol{xy},k+1}^-(\boldsymbol{S}_{\boldsymbol{y},k+1}^-\boldsymbol{S}_{\boldsymbol{y},k+1}^{-\intercal})^{-1}$$
$$\hat{\boldsymbol{x}}_{k+1}^+ = \hat{\boldsymbol{x}}_{k+1}^- + \boldsymbol{K}_{k+1}(\boldsymbol{y}_{k+1} - \hat{\boldsymbol{y}}_{k+1}^-)$$
$$\boldsymbol{S}_{\boldsymbol{x},k+1}^+ = \mathrm{QR}\left\{\left(\boldsymbol{S}_{\boldsymbol{x},k+1}^- - \boldsymbol{K}_{k+1}\boldsymbol{S}_{\boldsymbol{y}}^{(1)}\ \ \boldsymbol{K}_{k+1}\boldsymbol{S}_{\boldsymbol{y}}^{(2)}\ \ \boldsymbol{K}_{k+1}\sqrt{\boldsymbol{R}_\mathrm{w}}\right)\right\}$$

REFERENCES

Fox, J. (2007). *Robotergestützte Parameterschätzung für inertiale Messsysteme*. Logos, Berlin.

Kakabeeke, T., Roy, S., and Largo, R. (2006). Coordination training in individuals with incomplete spinal cord injury: consideration of motor hierachical structures. *Spinal Cord*, 44, 7–10.

Knestel, M. (2010). *MoreGait - Ein Rehabilitationsroboter zur Gangtherapie im Heimbereich*. Cuvillier, Göttingen.

Rupp, R., Plewa, H., Schuld, C., Gerner, H., Weidner, N., Hofer, E., and Knestel, M. (2011). Ein motorisiertes Exoskelett zur automatisierten Lokomotionstherapie im häuslichen Umfeld - Ergebnisse einer Pilotstudie mit inkomplett Querschnittgelähmten. *Neurol Rehabil*, 17(1), 13–20.

Specker, T., Buchholz, M., and Dietmayer, K. (2014). A new approach of dynamic friction modelling for simulation and observation. In *Proceedings of the 19th World Congress of The International Federation of Automatic Control, Cape Town, South Africa*.

van der Merwe, R. (2004). *Sigma-point Kalman filters for probabilistic inference in dynamic state-spacemodels*. Ph.D. thesis, Oregon Health & Science University.

Wirz, M., Zamon, D., Rupp, R., Scheel, A., Colombo, G., Dietz, V., and Hornby, T. (2005). Effetiveness of automated locomotor training in patients with chronic incomplete spinal cord injury: A multicenter trial. *Arch Phys Med Rehabil*, 86, 672–6780.